

Cross-composition Feature Disentanglement for Compositional Zero-shot Learning

Yuxia Geng¹, Runkai Zhu¹, Jiaoyan Chen², Jintai Chen³, Zhuo Chen⁴, Xiang Chen⁴, Can Xu¹,
Yuxiang Wang¹, Xiaoliang Xu¹

¹Hangzhou Dianzi University, ²The University of Manchester,
³University of Illinois at Urbana-Champaign, ⁴Zhejiang University

Abstract

Disentanglement of visual features of primitives (i.e., attributes and objects) has shown exceptional results in Compositional Zero-shot Learning (CZSL). However, due to the feature divergence of an attribute (resp. object) when combined with different objects (resp. attributes), it is challenging to learn disentangled primitive features that are general across different compositions. To this end, we propose the solution of *cross-composition feature disentanglement*, which takes multiple primitive-sharing compositions as inputs and constrains the disentangled primitive features to be general across these compositions. More specifically, we leverage a compositional graph to define the overall primitive-sharing relationships between compositions, and build a task-specific architecture upon the recently successful large pre-trained vision-language model (VLM) CLIP, with dual cross-composition disentangling adapters (called L-Adapter and V-Adapter) inserted into CLIP’s frozen text and image encoders, respectively. Evaluation on three popular CZSL benchmarks shows that our proposed solution significantly improves the performance of CZSL, and its components have been verified by solid ablation studies. Our code and data are available at: <https://anonymous.4open.science/t/DCDA-0BF7>.

Introduction

Compositional Zero-shot Learning (CZSL), which learns visual primitives from seen compositions of attributes and objects and combines them to recognize novel unseen compositions, has attracted extensive research interest in the past few years (Misra, Gupta, and Hebert 2017). For example, when presented with images of compositions like *red tomato* and *green apple*, the model could instantly recognize the new composition *green tomato* by combining the attribute *green* with the object *tomato*, even though it has never seen images of *green tomato*. This ability not only enables a deep neural network to tell plenty of new concepts with zero examples (Chen et al. 2023), but also facilitates the study of vision-language understanding (Chen et al. 2024) as the image features need to be accurately decomposed and recomposed with the guidance of textual attribute-object labels.

One solution for CZSL is to build a shared embedding space where the image features and the composition embeddings can be compared to perform classification (Wei

et al. 2019; Naeem et al. 2021; Mancini et al. 2022). Recently, its performance has been greatly improved by integrating large pre-trained vision-language models like CLIP (Radford et al. 2021) which jointly pre-trains an image encoder and a text encoder with visual-semantic alignment (Nayak, Yu, and Bach 2023). However, attributes and objects often highly depend on each other in images and their encoded visual features are too entangled to decompose. *Red tomato* is a typical example whose image pixels for *red* and *tomato* totally overlap. In view of this, recent CLIP-based methods either design separated soft prompts to learn disentangled textual features for attributes and objects and coax the model into identifying the single primitive in an image (Lu et al. 2023; Wang et al. 2023a), or insert trainable and parameter-independent adapters into the frozen image encoder to learn disentangled visual primitive features directly (Zheng, Zhu, and Nevatia 2024; Huang et al. 2024; Li et al. 2024). These disentangled representations enable finer-grained visual-semantic alignment at the primitive level.

However, the above methods treat the disentanglement of each composition independently, ignoring the **diversity** of attributes and objects across different compositions, i.e., an attribute (resp. object) tends to look greatly different when paired with different objects (resp. attributes); for example, in the compositions of *red apple*, *red tomato* and *red wine*, the attribute *red* is diverse e.g., the red tone ranges from shallow to deep. Such diversity may make the learned primitive features especially the visual ones less discriminative, thus limiting their generalization to their unseen compositions. In the left of Figure 1, we randomly sample some testing images whose annotated attributes have high diversity from the MIT-States dataset (Isola, Lim, and Adelson 2015), and visualize their disentangled attribute features of images learned by the previous state-of-the-art (SOTA) method CAILA (Zheng, Zhu, and Nevatia 2024). The disentangled features of images that share the same attribute mostly scatter in the vector space with limited discrimination. For example, the features of *broken* (purple circles) are fully mixed with the features of *cooked*, *coiled*, *mossy* and so on.

To obtain the disentangled primitive features that are more discriminative and general across different compositions (as in the right of Figure 1), we argue that introducing other compositions having the same attribute or object as the target composition during feature disentanglement

ment is beneficial. Inspired by (Naeem et al. 2021), we propose to utilize a compositional graph to define the overall primitive-sharing relationships between compositions, where all the attributes, objects, and compositions act as graph nodes and their compositional relationships are modeled by edges, as shown in the bottom of Figure 2(a). Based on this graph, we thereby propose **Dual Cross-composition Feature Decomposing Adapters (DCDA)** to augment the CLIP encoders on both language and vision sides so as to learn disentangled textual and visual representations of each primitive that are cross-composition generalizable.

Since the textual primitive features are less entangled than the visual primitive features due to the separated words in the label, DCDA has different implementations for the language and vision sides. Specifically, the adapter on the language side, called **L-Adapter**, applies a graph neural network (GNN) to the above compositional graph, to propagate the encoded textual features of neighboring compositions to an attribute or object node for its cross-composition generalizable primitive representation. Inspired by (Hao, Han, and Wong 2023), the adapter on the vision side, called **V-Adapter**, is first built upon the cross-attention between images of two primitive-sharing compositions (e.g., *red tomato* and *red wine*) to highlight the image features highly relevant to each other, i.e., the cross-composition generalizable features of their common primitive (e.g., *red*). Then, we propose a novel primitive-relevance-guided sampling strategy to effectively introduce more primitive-sharing compositions for more general primitive features, where two primitive graphs are extracted from the compositional graph to describe the attribute and object relevance. When integrating L-Adapters and V-Adapters into multiple layers of CLIP’s text and image encoders, we retain the original parameters of CLIP to avoid overfitting, but inject the task-specific knowledge. Our contributions can be summarized below:

- DCDA is among the first to investigate cross-composition feature disentanglement in CLIP-based CZSL, with the diversity of primitives concerned.
- A compositional graph and two derived primitive graphs are utilized to define exhaustive primitive-sharing compositions for less entangled text labels and more entangled image samples, respectively, with two kinds of effective adapters accordingly designed.
- DCDA achieves new SOTA results on MIT-States and UT-Zappos benchmarks in both *closed world* and *open world*, and has very competitive performance on C-GQA. Compared with CAILA, our method disentangles more clustered, more distinctive, and more generalizable attribute embeddings, as shown in the right of Figure 1. More details and comparisons on the disentangled object embeddings are attached in Appendix C.

Related Work

Conventional CZSL methods are roughly divided into two groups. One is classifier-based which first trains two separate classifiers to predict an input image’s attribute and object labels, respectively, and then combines them to predict the compositional labels (Misra, Gupta, and Hebert 2017;

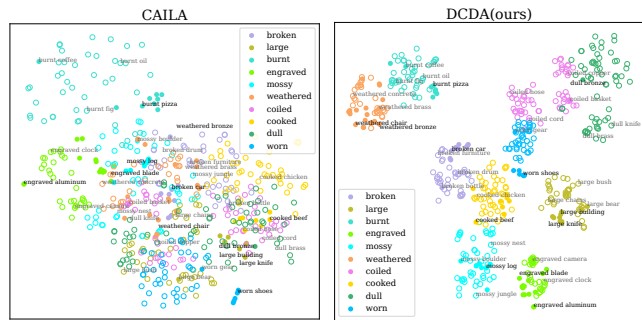


Figure 1: t -SNE visualizations of disentangled attribute representations of images in the test set of MIT-States, learned by CAILA (Zheng, Zhu, and Nevatia 2024) and our DCDA. Solid and hollow circles represent images of seen and unseen compositions, respectively. Best viewed in color.

Nagarajan and Grauman 2018). The subsequent works further propose to enhance the dependence of the attribute and object in a composition (Li et al. 2020, 2022; Wang et al. 2023b). The other group is embedding-based which jointly represents attributes and objects to capture the dependence, and then aligns them with the images in a shared embedding space (Wei et al. 2019; Karthik, Mancini, and Akata 2022). In particular, (Naeem et al. 2021) learn the joint representation through graph convolutional networks. There are also some works concerning the disentanglement of attribute and object features in the visual space (Saini, Pham, and Shrivastava 2022; Hao, Han, and Wong 2023; Kim et al. 2023). However, all these methods have to learn the alignment between image features and text embeddings from scratch and are prone to overfit to the seen compositions.

CLIP-based CZSL. After pre-training using 400 million image-text pairs, CLIP can be applied to any visual classification task without fine-tuning by setting prompts like “a photo of [class]”, where “[class]” is filled with the name of the class to be recognized. (Nayak, Yu, and Bach 2023) then had the first attempt to design prompt “a photo of [attribute] [object]” for CZSL, where “[attribute] [object]” are tunable tokens to teach CLIP how to compose attributes and objects.

To stress the roles of individual primitives, HPL (Wang et al. 2023a) additionally sets an attribute and an object prompt with only “[attribute]” or “[object]” tunable; DFSP (Lu et al. 2023) makes the whole prompt trainable and fuses the decomposed text features with the encoded (entangled) image features through a cross-modal fusion module. Different from these works focusing on optimizing the prompts, CAILA (Zheng, Zhu, and Nevatia 2024) proposes to insert trainable adapters inside the frozen transformer layers to decompose and recombine the attribute and object features. With disentangled primitive features, Troika (Huang et al. 2024) establishes three prediction branches and pulls a static class prompt to its dynamic images via a cross-modal traction module. (Li et al. 2024) investigate the relative specificity of attributes when paired with different objects. In contrast to these methods, our method DCDA is more general-

izable, with cross-composition knowledge injected and dual adapters inserted in CLIP’s image and text encoders.

Methodology

CZSL Task Formulation. Let $\mathcal{D}_{tr} = \{(x, c) | x \in \mathcal{X}_s, c \in \mathcal{C}_s\}$ be the training set, where \mathcal{X}_s contains the training images and \mathcal{C}_s is a set of seen compositional labels that are available during training. Each label is a tuple $c = (a, o)$ of an attribute class $a \in \mathcal{A}$ and an object class $o \in \mathcal{O}$. After training, the CZSL model can predict images of a set of new compositions \mathcal{C}_u that are unseen during training, with $\mathcal{C}_u \cap \mathcal{C}_s = \emptyset$. Following previous works, we study generalized CZSL (Purushwalkam et al. 2019), where images of seen and unseen compositions are both tested and the candidate label space includes both seen and unseen labels. The test set is thus denoted as $\mathcal{D}_{te} = \{(x, c) | x \in \mathcal{X}_{te}, c \in \mathcal{C}_{te}\}$, where $\mathcal{X}_{te} = \mathcal{X}_u \cup \mathcal{X}'_s$ with $\mathcal{X}'_s \cap \mathcal{X}_s = \emptyset$, and $\mathcal{C}_{te} = \mathcal{C}_u \cup \mathcal{C}_s$. Notably, \mathcal{C}_s and \mathcal{C}_u share the same attribute set \mathcal{A} and object set \mathcal{O} , CZSL assumes that each a and o has been trained before testing and only the composition $(a, o) \in \mathcal{C}_u$ is novel. **Overview.** In the following, we will first introduce the details of **L-Adapters** for the language side and **V-Adapters** for the vision side, and then introduce how to integrate them into the frozen CLIP encoders for CZSL. As shown in Figure 2(c), the adapters are inserted into CLIP’s intermediate computational units such as self-attention layers or feed-forward layers. This means the input of each adapter is the output of CLIP’s one computational unit, and its output is the input of CLIP’s next computational unit. We use $\mathbf{H}^t \in \mathbb{R}^{l \times d}$ and $\mathbf{H}^v \in \mathbb{R}^{l' \times d'}$ to denote the output of CLIP’s one specific computational unit in the text and image encoders, respectively, where l (resp. l') is the length of a tokenized input text (resp. image), d and d' is the hidden state size of each token.

The design of L-Adapter

Each L-Adapter is built upon a compositional graph for representing the global compositional relationships among attributes, objects and compositions, and a GNN module for propagating and aggregating features among them to realize the cross-composition learning of textual primitive features.

We first define the compositional graph. It consists of $N = |\mathcal{A}| + |\mathcal{O}| + |\mathcal{C}'|$ nodes, including all the attributes, all the objects, and the compositions in the current computation (i.e., $\mathcal{C}' = \mathcal{C}_s$ for training and $\mathcal{C}' = \mathcal{C}_{te}$ for testing). Given these nodes, for each $c = (a, o)$, we connect (a, o) , (a, c) and (o, c) to form a triangle in the graph, as shown in Figure 2(a). For simplicity and efficiency, we keep all graph edges unweighted and undirected as in (Naeem et al. 2021) and obtain a symmetric adjacency matrix $A \in \mathbb{R}^{N \times N}$ to store the graph structure, $A_{ij} = 1$ if there is a connection between node i and j otherwise $A_{ij} = 0$.

To obtain the initial representations of graph nodes, we first define individual prompts for attributes and objects as “a photo of [attribute] object” and “a photo of [object]” besides the composition prompts “a photo of [attribute] [object]”, then for each $c = (a, o)$, we feed three prompts into CLIP’s text encoder to output three hidden states \mathbf{H}_a^t , \mathbf{H}_o^t and \mathbf{H}_c^t for a, o, c , respectively, and finally extract the em-

beddings of the special token [EOT] in the prompts as the initial features $\{\mathbf{h}_i^t\}_{i=1}^N$ of graph nodes, with $\mathbf{h}_i^t = \mathbf{H}_{i, [\text{EOT}]}$ and $\mathbf{h}_i^t \in \mathbb{R}^d$. In this way, the text feature of each primitive is naturally disentangled from the composition one.

Next, we exploit multiple GNN layers to propagate features among graph nodes following the graph structure defined in A . Since many typical GNN models such as GCN (Kipf and Welling 2017), GAT (Velickovic et al. 2018) can be used here, we illustrate this procedure with two functions commonly defined in GNNs. One is AGG for aggregating features of one-hop neighbors for each node, and the other is CON for fusing the node feature and the neighborhood feature to make an update. Formally, as Figure 2(a)’s top shows, for each $c = (a, o)$, three identical AGG functions are parallelly applied to aggregate neighborhood features for nodes a, o, c at the k -th GNN layer, $k \in \{0, \dots, K - 1\}$, as:

$$\mathbf{a}_{\mathcal{N}_a^c}^{(k)} = \text{AGG}^{(k)}(\{\mathbf{c}_i^{(k)} | c_i \in \mathcal{N}_a^c\}, \{\mathbf{o}_i^{(k)} | o_i \in \mathcal{N}_a^o\}) \quad (1)$$

$$\mathbf{o}_{\mathcal{N}_o^c}^{(k)} = \text{AGG}^{(k)}(\{\mathbf{c}_j^{(k)} | c_j \in \mathcal{N}_o^c\}, \{\mathbf{a}_j^{(k)} | a_j \in \mathcal{N}_o^a\}) \quad (2)$$

$$\mathbf{c}_{c=(a,o)}^{(k)} = \text{AGG}^{(k)}(\mathbf{a}^{(k)}, \mathbf{o}^{(k)}) \quad (3)$$

where \mathcal{N}_a^c (resp. \mathcal{N}_o^c) denotes the composition neighbor set of a (resp. o) on the graph, and \mathcal{N}_a^o (resp. \mathcal{N}_o^a) includes the objects (resp. attributes) that compose the compositions in \mathcal{N}_a^c (resp. \mathcal{N}_o^c) together with a (resp. o). Considering the example in Figure 2(a) where $c = (a, o)$ is *red tomato*, \mathcal{N}_a^c includes compositions like *red apple* and \mathcal{N}_a^o includes objects like *apple*. While the neighbor set of each c only contains its primitives a and o . $\mathbf{a}^{(k)}$ is the input feature of a at the k -th layer, and is updated using CON function to obtain the k -th-layer output as $\mathbf{a}^{(k+1)} = \text{CON}(\mathbf{a}_{\mathcal{N}_a^c}^{(k)}, \mathbf{a}^{(k)})$, similar for o and c with outputs $\mathbf{o}^{(k+1)}$ and $\mathbf{c}^{(k+1)}$. The input feature of a, o, c at the first layer of GNN is the initialized node feature, e.g., $\mathbf{c}^{(0)} = \mathbf{h}_c^t$. The output features of a, o after K GNN layers $\mathbf{a}^{(K)}, \mathbf{o}^{(K)}$, which have already fused their neighboring compositions’ features, and c ’s output feature $\mathbf{c}^{(K)}$, which has aggregated the updated features of a and o , are the final output of one L-Adapter, and will be inputted into the next computation unit of CLIP for the latter computation.

The design of V-Adapter

Since attributes and objects are highly entangled within the input image, we cannot build the same computational graph in V-Adapters as that in L-Adapters. Targeting this, we leverage the cross-attention over primitive-sharing image pairs to extract cross-composition-sharing primitive features, and design a primitive relevance-guided sampling strategy to introduce more valid primitive-sharing compositions. We take disentangling attribute features from an input image as an example, object features are processed similarly.

Specifically, as shown in Figure 2(b), given a target image $x_{(a,o)}$ to predict, which is labeled by $c = (a, o)$, we first randomly sample an auxiliary composition that shares the same attribute as $x_{(a,o)}$ but has different object o' , and select one of its images $x_{(a,o')}$ as an auxiliary image. Then, we feed these two images into CLIP to output two hidden states $\mathbf{H}_{(a,o)}^v$ and $\mathbf{H}_{(a,o')}^v$ and compute the cross-attention as, with

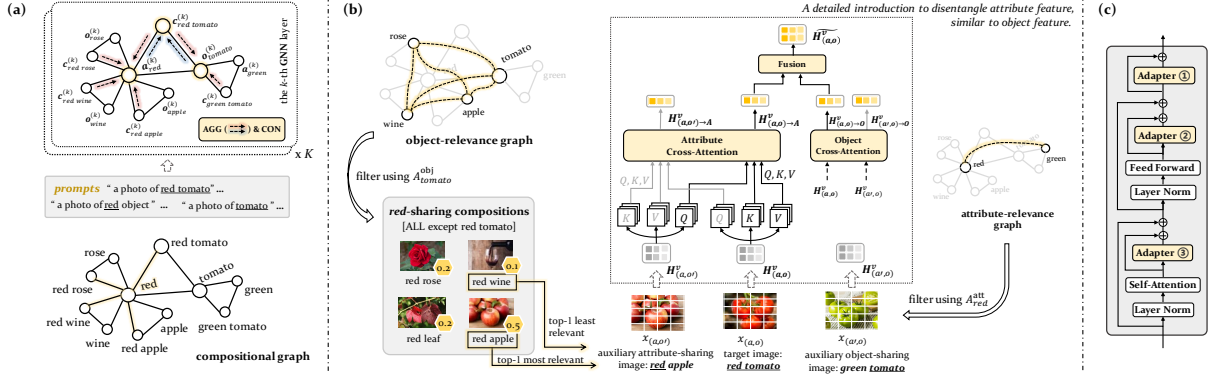


Figure 2: Overview of DCDA during training: (a) The L-Adapter built upon the composition graph and GNN module; (b) The V-adapter built upon the cross-attention and attribute/object relevance-guided sampling strategy; (c) An illustration of the candidate position for inserting adapters in a transformer block. We take the learning of *red tomato* as an example.

$H_{(a,o')}^v$ as the query and $H_{(a,o)}^v$ as the key and value:

$$\text{CrossAttention}(\mathbf{Q}, \mathbf{K}, \mathbf{V}) = \text{softmax}\left(\frac{\mathbf{Q}\mathbf{K}^T}{\sqrt{d'}}\right)\mathbf{V} \quad (4)$$

$$\mathbf{Q} = \mathbf{H}_{(a,o')}^v \mathbf{W}_Q, \mathbf{K} = \mathbf{H}_{(a,o)}^v \mathbf{W}_K, \mathbf{V} = \mathbf{H}_{(a,o)}^v \mathbf{W}_V \quad (5)$$

where $\mathbf{W}_{\{Q,K,V\}} \in \mathbb{R}^{d' \times d'}$ are three linear transformation matrices for flexible computation. We can see that every output embedding is a weighted sum of the value embeddings, and the weights are calculated by the similarity of the query and the key. By setting query as $H_{(a,o')}^v$, we can refine $H_{(a,o)}^v$ to keep features that are more specific to a , as well as attribute features that are general across these two compositions. We also swap the query and the value (also key) to refine $H_{(a,o')}^v$. The output of cross-attention is thus denoted as $H_{(a,o) \rightarrow A}^v$ and $H_{(a,o') \rightarrow A}^v$. A feed-forward layer is also added after the cross-attention.

Notably, the above cross-attention can only process two attribute-sharing compositions at one time. To introduce more compositions to learn more general attribute features, the model relies on the batched data and random sampling to switch the auxiliary composition. However, when an attribute is diverse with extensive composition neighbors, e.g., *broken*, which also means extensive candidate auxiliary compositions, the model requires more switches to traverse them, leading to inferior overall performance as shown in Table 1. To balance the switch times of attributes with different numbers of neighbors, we propose to select some representative compositions instead of all the compositions as the candidates, and for a target image $x_{(a,o)}$, the top- n objects that are most and least relevant to the target object o are paired with the target attribute a to serve as the representative (auxiliary) compositions, while the relevance between two objects can be determined by the number of common attributes that co-occur in their associated compositions in the training set; for example, if there are compositions *red tomato* and *red apple* in the training set, *red* is a common attribute of the objects *tomato* and *apple*.

To this end, we refer to the attribute-object edges in the training compositional graph to first create an *att-obj* graph

with structure matrix $A^{\text{att-obj}} \in \mathbb{R}^{|\mathcal{A}| \times |\mathcal{O}|}$, where $A_{i,j}^{\text{att-obj}} = 1$ means attribute i and object j form a valid seen composition while 0 not. Then, an object relevance graph can be created and its structure matrix is found as $A^{\text{obj}} = (A^{\text{att-obj}})^T A^{\text{att-obj}}$ with size $|\mathcal{O}| \times |\mathcal{O}|$, where $A_{j,j}^{\text{obj}}$ represents the number of common attributes between i -th and j -th objects, large numbers mean higher relevance. With this relevance graph, for target image $x_{(a,o)}$, and all of its a -sharing compositions besides (a, o) , denoted as $\{(a, o')\}$, we next refer to A_o^{obj} to obtain the relevance scores of objects in $\{o'\}$, and select the compositions whose objects have top- n maximum and top- n minimum non-zero scores as the representative compositions. Figure 2(b) presents a running example of this procedure. We perform a weighted random sampling over these representative compositions, i.e., the probability for selecting (a, o') is determined by the normalized relevance score between o' and o , more details are attached in Appendix A.

The same applies to the output of the object cross-attention $H_{(a,o) \rightarrow O}^v$, which is learned from a set of representative o -sharing compositions selected by referring to the attribute relevance matrix $A_a^{\text{att}} = A^{\text{att-obj}}(A^{\text{att-obj}})^T$ and its row value A_a^{att} . In this way, we learn the cross-composition-sharing primitive features of an input image, and have the updated image features: $\widehat{H}_{(a,o)}^v = H_{(a,o) \rightarrow A}^v + H_{(a,o) \rightarrow O}^v$, which will be taken as the final output of one V-Adapter together with $H_{(a,o) \rightarrow A}^v$ and $H_{(a,o) \rightarrow O}^v$.

Integrating Adapters into CLIP

Given a single L-Adapter and V-Adapter, we next present how to insert them into two connected computation units in CLIP. Inspired by ViT (Dosovitskiy et al. 2020) which tends to learn general features at lower layers and learn specific features at higher layers, we add our adapters starting from the top transformer blocks. After preliminary validations on MIT-States (see our Ablation Study results for more), we decided to *i*) insert adapters at the last three transformer blocks of both text and image encoders, and *ii*) add L-Adapters behind the self-attention layer and feed-forward layer in each language transformer block (i.e., the positions ③ and ② in

Figure 2(c)), and attach V-Adapters after the whole vision transformer block (i.e., the position ① in Figure 2(c)). Moreover, we build a skip connection between the input and the output of each adapter before inputting it into the next computation unit of CLIP. We use CLIP’s pre-trained word embeddings to initialize each word in our prompts, including the prefix words “a photo of”, and keep these word embeddings trainable for capturing more task-specific knowledge.

Training and Inference

At the last transformer blocks, we obtain the output of L-Adapter and V-Adapter after skip connection, denoted as \widehat{H}^v and \widehat{H}^t , based on this, we extract the embeddings of [EOT] token, i.e., $\widehat{h}^v (= \widehat{H}_{[\text{EOT}]}^v)$ and $\widehat{h}^t (= \widehat{H}_{[\text{EOT}]}^t)$, to measure the compatibility of visual and textual features. Formally, for an input image x_i and a training composition $c_i = (a_i, o_i)$, we compute the compatibility score as:

$$s(x_i, c_i = (a_i, o_i)) = \alpha [\widehat{h}_i^v \cdot \widehat{h}_{c_i}^t] + \beta [\widehat{h}_{i \rightarrow A}^v \cdot \widehat{h}_{a_i}^t] + \gamma [\widehat{h}_{i \rightarrow O}^v \cdot \widehat{h}_{o_i}^t] \quad (6)$$

where we also measure the individual primitive compatibility via the second and the third items as if one image belongs to an attribute-object pair, its disentangled attribute and object features also belong to the corresponding primitive labels. We use three learnable parameters α, β, γ to balance the overall score. \cdot denotes the dot-product similarity.

We optimize these adapters and trainable token embeddings by minimizing the cross-entropy loss on the training set \mathcal{D}_{tr} with seen compositions from \mathcal{C}_s :

$$\mathcal{L} = -\frac{1}{|\mathcal{D}_{tr}|} \sum_{x_i \in \mathcal{D}_{tr}} \log \frac{e^{[s(x_i, c_i = (a_i, o_i)) / \tau]}}{\sum_{c_j \in \mathcal{C}_s} e^{[s(x_i, c_j = (a_j, o_j)) / \tau]}} \quad (7)$$

where τ is the temperature commonly used in CLIP, $c_i = (a_i, o_i)$ is expected to be the ground-truth label.

During inference, for each testing image x_t , we estimate the compatibility score between x_t and each testing composition $c = (a, o)$ from \mathcal{C}_{te} as Equation 6. The composition that has the highest compatibility score is the predicted label. Besides, since we have no idea about the attribute and object labeled for the testing image, we take itself as the primitive-sharing images for computing $H_{t \rightarrow A}^v$ and $H_{t \rightarrow O}^v$.

Experiments

Experimental Settings

Datasets and Metrics We experiment with three popular benchmarks for CZSL: MIT-States (Isola, Lim, and Adelson 2015), UT-Zappos (Yu and Grauman 2014) and C-GQA (Naeem et al. 2021), and follow (Purushwalkam et al. 2019; Naeem et al. 2021) to split the data for training, validation and testing. For each dataset, we compute the prediction accuracy of seen and unseen compositions, and report four metrics: the best Seen (**S**) and Unseen (**U**) accuracy, the best harmonic mean (**H**), and the Area Under the accuracy Curve (**AUC**). Among them, AUC is the most comprehensive one and is widely adopted as the core metric by previous works (Purushwalkam et al. 2019; Zheng, Zhu, and Nevatia 2024). Please see Appendix B for more datasets and metrics details.

Closed World and Open World Settings Given the attribute set \mathcal{A} and object set \mathcal{O} , the complete compositional label set \mathcal{C} should be the Cartesian product of \mathcal{A} and \mathcal{O} , i.e., $\mathcal{C} = \mathcal{A} \times \mathcal{O}$ with size $|\mathcal{A}| \times |\mathcal{O}|$. However, current benchmarks often operate in a *closed world* setting where unseen compositions \mathcal{C}_u in \mathcal{C}_{te} are a small subset of $\mathcal{C} \setminus \mathcal{C}_s$ and are assumed to be known. For example, MIT-States contains 28,175 possible compositions with 115 attributes and 245 objects, but the label space for testing is limited to 1,962 compositions (1,262 seen and 700 unseen), covering less than 7% of the complete set. Thus, we follow (Mancini et al. 2021) to evaluate our model in the *open world* setting, where the testing images remain unchanged but the testing label space is all possible combinations, i.e., $\mathcal{C}_{te} = \mathcal{C}$ and $\mathcal{C}_u = \mathcal{C} \setminus \mathcal{C}_s$, which is more challenging as the models have to generalize from a small set of seen to a very large set of unseen compositions. Notably, not all the combinations are feasible, such as *eroded cat*, for this, we apply post-training calibration (Nayak, Yu, and Bach 2023; Xu, Chai, and Kordjamshidi 2024) to filter out unreasonable compositions.

Baselines and Model Variants We mainly compare our DCDA with the existing CLIP-based CZSL methods, including the vanilla CLIP without fine-tuning, CSP (Nayak, Yu, and Bach 2023), HPL (Wang et al. 2023a), DFSP (Lu et al. 2023), GIPCOL (Xu, Chai, and Kordjamshidi 2024), CAILA (Zheng, Zhu, and Nevatia 2024), and Troika (Huang et al. 2024). We also include two non-CLIP-based baselines that are most similar to us, namely CGE (Naeem et al. 2021) and ADE (Hao, Han, and Wong 2023).

In V-Adapters, we propose a novel primitive-relevance guided (PRG) sampling method to select representative auxiliary compositions to sample rather than performing purely random (RD) sampling over all neighboring compositions. For detailed comparisons, we develop a variant DCDA[RD] and denote the vanilla model as DCDA[PRG]. Given the imbalanced sample distribution, we also focus on the tail compositions in the neighbor set, and sample them according to the reciprocal of their image numbers (N) to supply DCDA[PRG], leading to a new variant DCDA[PRG+N], these two sampling strategies are switched batch by batch.

Implementation Details We implement our models with PyTorch and use Adam as the optimizer, with the learning rate set to 5e-5, 5e-5, 1e-5, and the batch size set to 32, 32, 16 for MIT-States, UT-Zappos, C-GQA, respectively, the weight decay is set to 5e-5 for all datasets. The GNN module is implemented as GCN with $K = 2$. n for selecting the representative auxiliary compositions is set to 5. The initialized value of α, β, γ are all set to 1, and later optimized together with other parameters. The optimum configurations w.r.t these hyper-parameters are determined by AUC on the validation set. All the experiments are run on a single NVIDIA Tesla A100 GPU with 40GB memory.

Main Results

The overall prediction results in *closed world* are reported in the top section of Table 1. It can be seen that our models DCDA[PRG] and DCDA[PRG+N] always outperform

Setting	Methods	MIT-States				UT-Zappos				C-GQA			
		S	U	H	AUC	S	U	H	AUC	S	U	H	AUC
Closed World	CGE	32.8	28.0	21.4	6.5	64.5	71.5	60.5	33.5	33.5	15.5	16.0	4.2
	ADE	–	–	–	–	–	–	–	–	35.0	17.7	18.0	5.2
	CLIP	30.2	46.0	26.1	11.0	15.8	49.1	15.6	5.0	7.5	25.0	8.6	1.4
	CSP	46.6	49.9	36.3	19.4	64.2	66.2	46.6	33.0	28.8	26.8	20.5	6.2
	HPL	47.5	50.6	37.3	20.2	63.0	68.8	48.2	35.0	30.8	28.4	22.4	7.2
	GIPCOL	48.5	49.6	36.6	19.9	65.0	68.5	48.8	36.2	31.9	28.4	22.5	7.14
	DFSP	46.9	52.0	37.3	20.6	66.7	71.7	47.2	36.0	<i>37.3</i>	<i>26.1</i>	<i>23.5</i>	8.2
	CAILA	51.0	53.9	39.9	23.4	67.8	<u>74.0</u>	57.0	<u>44.1</u>	40.4	<u>28.6</u>	26.1	9.9
	Troika	49.0	53.0	39.3	22.1	66.8	73.8	54.6	41.7	<i>38.0</i>	<i>28.4</i>	<i>25.3</i>	9.2
	DCDA[RD]	42.2	46.7	32.8	16.2	64.7	71.5	54.5	40.1	<u>39.8</u>	25.3	<u>23.9</u>	8.5
DCDA[PRG]	57.3	<u>55.1</u>	43.2	<u>26.9</u>	<u>68.7</u>	72.4	56.5	43.0	<u>39.1</u>	26.7	24.5	8.9	
DCDA[PRG+N]	<u>57.1</u>	55.5	<u>43.1</u>	27.0	69.1	74.1	<u>57.2</u>	44.2	<u>38.5</u>	28.8	<u>25.3</u>	<u>9.4</u>	
Open World	CGE	32.4	5.1	6.0	1.0	61.7	47.7	39.0	23.1	32.1	1.8	2.9	0.47
	ADE	–	–	–	–	–	–	–	–	35.1	4.8	7.6	1.42
	CLIP	30.1	14.3	12.8	3.0	15.7	20.6	11.2	2.2	7.5	4.6	4.0	0.27
	CSP	46.3	15.7	17.4	5.7	64.1	44.1	38.9	22.7	28.7	5.2	6.9	1.20
	HPL	46.4	18.9	19.8	6.9	63.4	48.1	40.2	24.6	30.1	5.8	7.5	1.37
	GIPCOL	48.5	16.0	17.9	6.3	65.0	45.0	40.1	23.5	31.6	5.5	7.3	1.30
	DFSP	47.5	18.5	19.3	6.8	66.8	60.0	44.0	30.3	35.0	4.9	7.3	1.42
	CAILA	51.0	20.2	21.6	8.2	<u>67.8</u>	59.7	49.4	32.8	40.4	6.6	9.6	2.26
	Troika	48.8	18.7	20.1	7.2	66.4	<u>61.2</u>	47.8	33.0	<i>37.4</i>	4.5	6.0	1.11
	DCDA[PRG]	<u>54.6</u>	<u>27.3</u>	<u>25.8</u>	<u>11.5</u>	68.6	56.4	<u>51.2</u>	<u>33.8</u>	35.5	4.4	6.7	1.30
DCDA[PRG+N]	55.0	27.7	26.7	12.0	67.8	62.5	51.4	35.8	35.3	6.4	<u>8.5</u>	<u>1.76</u>	

Table 1: Overall Results (%) on three benchmarks. In each setting, the best results are in bold and the second best are underlined. We report DFSP in its *t2i* setting. Numbers in italics mean the results implemented with CLIP-base, others are with CLIP-large.

the baselines of both non-CLIP-based and CLIP-based. Especially, on MIT-States, DCDA[PRG] and DCDA[PRG+N] achieved the top-2 best results and have been the new SOTA, on all metrics. They outperform the previous SOTA CAILA by a large margin, with over 3% improvements on both AUC and H, and over 6% improvements on seen accuracy.

On UT-Zappos, DCDA[PRG+N] is the best with 3 out of 4 metrics. Despite the inferior results on H compared with CGE, it beats CGE a lot on the core metric AUC. In contrast to the slight performance gap between DCDA[PRG+N] and DCDA[PRG] on MIT-States, DCDA[PRG+N] shows great superiority on UT-Zappos, which is consistent with the fact that UT-Zappos is a more imbalanced dataset (the standard deviation of its sample size for all classes is ~ 465 , which is larger than that of MIT-States (~ 12) and C-GQA (~ 22)).

In our preliminary experiments, we found our models underperform the previous SOTA CAILA on C-GQA. This may be because the images in C-GQA have a lower resolution and smaller sizes, which might require more task-specific parameters to fit, just as CAILA inserts adapters into all the transformer layers in CLIP, while we only insert into the last three layers. To this end, after multiple attempts, we finally decided to freeze the image encoder to fully update its parameters together with our V-Adapters (please see Table 5 in Appendix B for more). The resulting DCDA[PRG] and DCDA[PRG+N] eventually achieved very competitive results against CAILA, as Table 1 shows. Here, to afford more trainable parameters, we run our models and some baselines with CLIP-base on C-GQA, while on MIT-States and UT-Zappos, we still follow previous works to use CLIP-large.

Compared with DCDA[RD], DCDA[PRG] achieves great outperformance on all datasets, indicating the effectiveness of our proposed primitive-relevance guided sampling strate-

gies. Especially, the improvement on MIT-States is promising, since the number of compositions surrounding its each primitive is more imbalanced than that of UT-Zappos. Although C-GQA is also more imbalanced, the improvement is limited by its low-quality and small-size image samples.

Among all CLIP-based methods, CAILA, Troika and our DCDA are the only three that propose to insert trainable adapters into CLIP’s image encoder to learn disentangled image features, and achieve the top-3 best results on all datasets with significant improvements over other methods. This indicates the disentanglement of visual primitive features plays a key role in CZSL, which also facilitates more effective solutions to adapt CLIP to the CZSL task well, such as Troika’s multi-path solution. Also, our method consistently beats CAILA and Troika on both the general dataset MIT-States and the domain-specific dataset UT-Zappos. The comparable results on C-GQA also motivate us to develop more advanced learning paradigms in the future.

Table 1’s bottom section records the results in *open world*, from which we have similar observations as in *closed world*: our method achieves new SOTA on MIT-States and UT-Zappos, and is still the second best on C-GQA, illustrating that our method has a good generalization ability even though the unseen label space is extremely enlarged.

Effectiveness of Adapters

The whole Adapters We evaluate the contribution of L-Adapter and V-Adapter by analyzing the performance drop when one of them is removed. Notably, when all L-Adapters (reps. V-Adapters) are removed, the text (resp. image) encoder will act like CLIP’s default frozen encoders to output an entangled representation for each input prompt (resp. image). We conduct experiments on MIT-States dataset under

Models	S	U	H	AUC
Full Model (e.g., DCDA[PRG])	57.3	55.1	43.2	26.9
w/o L-Adapters	55.9	54.7	42.2	26.1
w/o V-Adapters	44.9	46.9	33.8	17.1
L-Adapter w/o other compositions	57.5	54.6	43.0	26.7
V-Adapter w/o other compositions	44.5	46.2	33.7	17.0
L&V-Adapter w/o other compositions	44.2	46.1	33.6	16.7

Table 2: Adapter Analysis on MIT-States in *closed world*.

the *closed world* setting, the results are shown in the second and third lines of Table 2. We can see that the performance both declines when L-Adapters or V-Adapters are removed, indicating that they two both have a positive contribution to the DCDA model and are complementary to each other. We also observe that the performance decrease of removing V-Adapters is greater than that of removing L-Adapters, which is consistent with our statement: textual primitive features are less entangled than visual ones, and the independent textual primitive features can still be captured by setting individual primitive prompts.

Cross-composition Information in Adapters We further validate the effectiveness of introducing primitive-sharing compositions for each target composition by deleting the compositional graph in L-Adapters and/or auxiliary compositions in V-Adapters. Concretely, we merely keep the prompts’ token embeddings trainable in L-Adapters; and/or replace the two auxiliary images with the target image itself in V-Adapters, which thus turns into the self-attention on the input image, but still projects the primitive features into different subspaces with different attention networks. The results on MIT-States are shown in the last three lines of Table 2. The performance drop indicates the superiority of introducing primitive-sharing compositions in both text and image encoders. In particular, we find that V-Adapters without primitive-sharing compositions even perform worse than removing the whole V-Adapters, illustrating that these compositions play a considerable role in constraining the learning of primitive features in different subspaces. In contrast, L-Adapters without neighboring (primitive-sharing) compositions perform better than removing the whole L-Adapters. However, the performance gap is slight, which may be attributed to that we also set the embeddings of tokens in the prompts tunable, the cross-composition primitive features can be implicitly captured by optimizing the token embeddings with multiple samples.

Ablation Studies

We also ablate our model w.r.t the insertion location and depth of Adapters on MIT-States in *closed world*.

Insertion Location of Adapters There are two choices for inserting adapters into a transformer block, i.e., inside or outside. Therefore, we experiment with four configurations where every L-Adapter and V-Adapter are added inside or outside a transformer block, as shown in Table 3. Notably, the inside insertion includes adding after the self-attention and feed-forward layers in a block, i.e., the positions ③ and ② in Figure 2(c). From Table 3, it can be seen that adding

L-Adapters		V-Adapters		MIT-States			
I	O	I	O	S	U	H	AUC
✓		✓		53.5	53.4	40.6	24.0
✓			✓	57.3	55.1	43.2	26.9
	✓	✓		53.1	53.0	41.0	24.0
	✓		✓	56.0	55.5	43.2	26.7

Table 3: Ablation Study on Adapters’ Insertion Locations, i.e., inside (I) or outside (O) one transformer block.

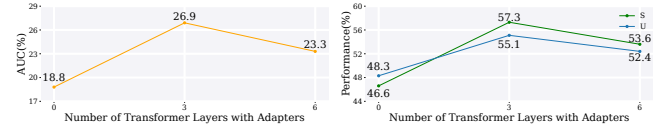


Figure 3: Performance (AUC, S and U) of increasing the number of transformer layers with adapters on MIT-States.

V-Adapters outside transformer layers often achieves better performance no matter where L-Adapters are located, while there is no significant difference when shifting L-Adapters at different positions. This may be because when adding a V-Adapter inside the transform layer, there is no nonlinear transformation like Feed-Forward layer between two attention operations for extracting more informative features. Regarding the better performance with inside L-Adapters and outside V-Adapters, we finally apply this configuration to three benchmarks.

Insertion Depth of Adapters We further show the performance change when we increase the number of transformer blocks with trainable adapters in Figure 3. As mentioned earlier, we start from the top transformer layers. It is clear that the best performance is achieved with the last 3 layers, while the last 6 layers may overfit the training data, with less generalization knowledge from our adapters and CLIP.

Conclusions and Outlook

In this study, we proposed DCDA, a novel CLIP-based CZSL method, which includes dual trainable adapters (i.e., L-Adapters and V-Adapters) inserted into the frozen text and image encoders of CLIP for learning textual and visual cross-composition disentangled representations for attribute and object primitives in CZSL. Specifically, L-Adapters are built upon a compositional graph with features of different composition neighbors aggregated to their centric attributes or objects, while V-Adapters are built upon the cross-attention over multiple primitive-sharing compositions with a sampling strategy guided by two primitive-relevance graphs. Unlike the disentangled primitive features learned previously, we derive more discriminative and more general primitive features, with promising results achieved on three popular benchmarks. Moreover, in our experiments, we find that the performance gain is mostly from V-Adapters, illustrating the serious entanglement of primitive features in the image data. While the entanglement of textual primitive features is also noticeable as the incorporation of L-Adapters leads to better performance. In the future, it is

expected to apply our dual adapters in other vision-language tasks such as visual question answering (Chen et al. 2021) and image captioning (Vinyals et al. 2015).

References

- Chen, J.; Geng, Y.; Chen, Z.; Pan, J. Z.; He, Y.; Zhang, W.; Horrocks, I.; and Chen, H. 2023. Zero-shot and few-shot learning with knowledge graphs: A comprehensive survey. *Proceedings of the IEEE*, 653–685.
- Chen, Z.; Chen, J.; Geng, Y.; Pan, J. Z.; Yuan, Z.; and Chen, H. 2021. Zero-shot visual question answering using knowledge graph. In *20th International Semantic Web Conference, ISWC 2021, Proceedings 20*, 146–162. Springer.
- Chen, Z.; Zhang, Y.; Fang, Y.; Geng, Y.; Guo, L.; Chen, X.; Li, Q.; Zhang, W.; Chen, J.; Zhu, Y.; et al. 2024. Knowledge Graphs Meet Multi-Modal Learning: A Comprehensive Survey. *arXiv preprint arXiv:2402.05391*.
- Dosovitskiy, A.; Beyer, L.; Kolesnikov, A.; Weissenborn, D.; Zhai, X.; Unterthiner, T.; Dehghani, M.; Minderer, M.; Heigold, G.; Gelly, S.; et al. 2020. An image is worth 16x16 words: Transformers for image recognition at scale. *arXiv preprint arXiv:2010.11929*.
- Hao, S.; Han, K.; and Wong, K.-Y. K. 2023. Learning attention as disentangler for compositional zero-shot learning. In *Proceedings of the IEEE/CVF Conference on Computer Vision and Pattern Recognition*, 15315–15324.
- Huang, S.; Gong, B.; Feng, Y.; Zhang, M.; Lv, Y.; and Wang, D. 2024. Troika: Multi-path cross-modal traction for compositional zero-shot learning. In *Proceedings of the IEEE/CVF Conference on Computer Vision and Pattern Recognition*, 24005–24014.
- Hudson, D. A.; and Manning, C. D. 2019. Gqa: A new dataset for real-world visual reasoning and compositional question answering. In *Proceedings of the IEEE/CVF conference on computer vision and pattern recognition*, 6700–6709.
- Isola, P.; Lim, J. J.; and Adelson, E. H. 2015. Discovering states and transformations in image collections. In *Proceedings of the IEEE conference on computer vision and pattern recognition*, 1383–1391.
- Karthik, S.; Mancini, M.; and Akata, Z. 2022. Kg-sp: Knowledge guided simple primitives for open world compositional zero-shot learning. In *Proceedings of the IEEE/CVF Conference on Computer Vision and Pattern Recognition*, 9336–9345.
- Kim, H.; Lee, J.; Park, S.; and Sohn, K. 2023. Hierarchical visual primitive experts for compositional zero-shot learning. In *Proceedings of the IEEE/CVF International Conference on Computer Vision*, 5675–5685.
- Kipf, T. N.; and Welling, M. 2017. Semi-Supervised Classification with Graph Convolutional Networks. In *5th International Conference on Learning Representations, ICLR 2017, Toulon, France, April 24-26, 2017, Conference Track Proceedings*. OpenReview.net.
- Li, X.; Yang, X.; Wei, K.; Deng, C.; and Yang, M. 2022. Siamese contrastive embedding network for compositional zero-shot learning. In *Proceedings of the IEEE/CVF conference on computer vision and pattern recognition*, 9326–9335.
- Li, Y.; Liu, Z.; Chen, H.; and Yao, L. 2024. Context-based and Diversity-driven Specificity in Compositional Zero-Shot Learning. In *Proceedings of the IEEE/CVF Conference on Computer Vision and Pattern Recognition*, 17037–17046.
- Li, Y.-L.; Xu, Y.; Mao, X.; and Lu, C. 2020. Symmetry and group in attribute-object compositions. In *Proceedings of the IEEE/CVF Conference on Computer Vision and Pattern Recognition*, 11316–11325.
- Lu, X.; Guo, S.; Liu, Z.; and Guo, J. 2023. Decomposed soft prompt guided fusion enhancing for compositional zero-shot learning. In *Proceedings of the IEEE/CVF Conference on Computer Vision and Pattern Recognition*, 23560–23569.
- Mancini, M.; Naeem, M. F.; Xian, Y.; and Akata, Z. 2021. Open world compositional zero-shot learning. In *Proceedings of the IEEE/CVF conference on computer vision and pattern recognition*, 5222–5230.
- Mancini, M.; Naeem, M. F.; Xian, Y.; and Akata, Z. 2022. Learning graph embeddings for open world compositional zero-shot learning. *IEEE Transactions on pattern analysis and machine intelligence*.
- Misra, I.; Gupta, A.; and Hebert, M. 2017. From red wine to red tomato: Composition with context. In *Proceedings of the IEEE Conference on Computer Vision and Pattern Recognition*, 1160–1169.
- Naeem, M. F.; Xian, Y.; Tombari, F.; and Akata, Z. 2021. Learning graph embeddings for compositional zero-shot learning. In *Proceedings of the IEEE/CVF Conference on Computer Vision and Pattern Recognition*, 953–962.
- Nagarajan, T.; and Grauman, K. 2018. Attributes as operators: factorizing unseen attribute-object compositions. In *Proceedings of the European Conference on Computer Vision (ECCV)*, 172–190.
- Nayak, N. V.; Yu, P.; and Bach, S. H. 2023. Learning to Compose Soft Prompts for Compositional Zero-Shot Learning. In *The Eleventh International Conference on Learning Representations, ICLR 2023*.
- Purushwalkam, S.; Nickel, M.; Gupta, A.; and Ranzato, M. 2019. Task-driven modular networks for zero-shot compositional learning. In *Proceedings of the IEEE/CVF International Conference on Computer Vision*, 3592–3601.
- Radford, A.; Kim, J. W.; Hallacy, C.; Ramesh, A.; Goh, G.; Agarwal, S.; Sastry, G.; Askell, A.; Mishkin, P.; Clark, J.; et al. 2021. Learning transferable visual models from natural language supervision. In *International conference on machine learning*, 8748–8763. PMLR.
- Saini, N.; Pham, K.; and Shrivastava, A. 2022. Disentangling visual embeddings for attributes and objects. In *Proceedings of the IEEE/CVF Conference on Computer Vision and Pattern Recognition*, 13658–13667.
- Velickovic, P.; Cucurull, G.; Casanova, A.; Romero, A.; Liò, P.; and Bengio, Y. 2018. Graph Attention Networks. In *6th International Conference on Learning Representations, ICLR 2018, Conference Track Proceedings*.

- Vinyals, O.; Toshev, A.; Bengio, S.; and Erhan, D. 2015. Show and tell: A neural image caption generator. In *Proceedings of the IEEE conference on computer vision and pattern recognition*, 3156–3164.
- Wang, H.; Yang, M.; Wei, K.; and Deng, C. 2023a. Hierarchical prompt learning for compositional zero-shot recognition. In *Proceedings of the Thirty-Second International Joint Conference on Artificial Intelligence*, 1470–1478.
- Wang, Q.; Liu, L.; Jing, C.; Chen, H.; Liang, G.; Wang, P.; and Shen, C. 2023b. Learning conditional attributes for compositional zero-shot learning. In *Proceedings of the IEEE/CVF Conference on Computer Vision and Pattern Recognition*, 11197–11206.
- Wei, K.; Yang, M.; Wang, H.; Deng, C.; and Liu, X. 2019. Adversarial fine-grained composition learning for unseen attribute-object recognition. In *Proceedings of the IEEE/CVF International Conference on Computer Vision*, 3740–3748.
- Xu, G.; Chai, J.; and Kordjamshidi, P. 2024. GIPCOL: Graph-Injected Soft Prompting for Compositional Zero-Shot Learning. In *Proceedings of the IEEE/CVF Winter Conference on Applications of Computer Vision*, 5774–5783.
- Yu, A.; and Grauman, K. 2014. Fine-grained visual comparisons with local learning. In *Proceedings of the IEEE conference on computer vision and pattern recognition*, 192–199.
- Zheng, Z.; Zhu, H.; and Nevatia, R. 2024. CAILA: Concept-Aware Intra-Layer Adapters for Compositional Zero-Shot Learning. In *Proceedings of the IEEE/CVF Winter Conference on Applications of Computer Vision*, 1721–1731.

Appendix

A. Supplementary Methodology Details

Computing the Sampling Probability To sample the top- n most and least relevant compositions according to the top- n maximum and minimum primitive relevance scores, we take two different ways to compute the sampling probabilities. More specifically, the probability for selecting the top- n most relevant compositions, e.g., (a, o'_i) , is computed as:

$$P(o' = o'_i) = \frac{A_{o, o'_i}^{\text{obj}}}{\sum_{o'_k \in \{o'\}} A_{o, o'_k}^{\text{obj}}},$$

where A_{o, o'_i}^{obj} means the relevance score between objects o'_i and o , while the probability for selecting the top- n least relevant compositions, e.g., (a, o'_j) , is computed as:

$$P(o' = o'_j) = -\frac{A_{o, o'_j}^{\text{obj}}}{\sum_{o'_k \in \{o'\}} A_{o, o'_k}^{\text{obj}}}.$$

The difference is that the n normalized minimum scores are multiplied by -1 to ensure that the top-1 least relevant composition has the highest probability of being sampled among the n least relevant compositions. Consider the example in Figure 2(b), *red wine*, *red rose* and *red leaf* are top-3 least relevant compositions for *red tomato*, with top-3 normalized minimum object-relevance scores: 0.1, 0.2 and 0.2, respectively, while *red wine* is the top-1 least relevant composition with the highest sampling probability among these three compositions.

To avoid being confused by the positive and negative sampling probabilities, we divide the representative compositions into two groups and sample over the top- n most and least relevant compositions independently. To be more specific, we switch them batch by batch.

B. Supplementary Experiment Details

Dataset MIT-States contains 53,753 real-world images, annotated by a variety of classes with 245 objects and their 115 attributes in the general domain. In *closed world*, it provides 1,962 compositions in total, 1,262 of which are seen used for training, and 700 are unseen with 300 for validation and 400 for testing. UT-Zappos is a more domain-specific dataset, containing 50,025 images of shoes paired with their material attributes. In total, it has 16 attributes and 12 objects, yielding 83 seen and 33 unseen compositions under the *closed world* setting. C-GQA, derived from of Stanford GQA dataset (Hudson and Manning 2019), is the most extensive dataset for CZSL, containing 7,767 compositions (5,592/2,175 as seen/unseen), 413 attribute classes, 674 object classes, and 39,298 images in total. Table 4 summarizes the statistics of these three datasets in the *closed world* setting, the *open world* has the same set of testing images, i.e., \mathcal{X}_{te} , but larger candidate label set, i.e., all possible compositions \mathcal{C} obtained by the Cartesian product of \mathcal{A} and \mathcal{O} .

Evaluation Metrics We compute the prediction accuracy for recognizing seen and unseen compositions, i.e., the generalized CZSL, in both *closed world* and *open world* scenarios. Specifically, due to the inherent bias towards seen

Datasets	Composition \mathcal{A} / \mathcal{O}	Train		Validation		Test	
		\mathcal{C}_s	\mathcal{X}_s	\mathcal{C}_v / \mathcal{C}_s	\mathcal{X}_{va}	\mathcal{C}_t / \mathcal{C}_v	\mathcal{X}_t
MIT-States	115 / 245	1,262	30,338	300 / 300	10,420	400 / 400	12,995
UT-Zappos	16 / 12	83	22,998	15 / 15	3,214	18 / 18	2,914
C-GQA	413 / 674	5,592	26,920	1,040 / 1,252	7,280	888 / 923	5,098

Table 4: Statistics of Datasets for CZSL. $|\mathcal{C}_u|$ here is the number of unseen compositions in the *closed world* setting.

classes, we follow the current standard (Purushwalkam et al. 2019; Nayak, Yu, and Bach 2023) to add a scalar bias to the prediction scores of unseen classes and vary the bias from $-\infty$ to $+\infty$ to get a seen-unseen accuracy curve, which indicates the seen accuracy on the x-axis and unseen accuracy on the y-axis. Correspondingly, we can report the best seen accuracy (S), where the bias is set to $-\infty$ and the models only predict on the seen labels, and report the best unseen accuracy (U), where the bias is set to $+\infty$ and the models only predict on the unseen labels. Also, we calculate the best harmonic mean (H), where a harmonic mean value is first computed for each point on the curve to balance the seen accuracy (acc_s) and unseen accuracy (acc_u) as $(2 \times acc_s \times acc_u) / (acc_s + acc_u)$, and then the highest value across all the selected points is reported. Finally, we compute the Area Under the accuracy Curve (AUC) as a comprehensive metric.

Experiments on C-GQA To deal with the low-resolution and small-size images in C-GQA, we tried to add more trainable adapters in CLIP’s image encoder or fully fine-tune the whole image encoder, to adapt CLIP to this kind of image. More specifically, we add a downsample-upsample style adapter, which is similar to the adapter used in CAILA and Troika, after the self-attention layer and feed-forward layer in each vision transformer block (i.e., the positions ③ and ② in Figure 2(c)), except for the last three transformer blocks where our V-Adapters have already been there. In addition, we also try to freeze the whole image encoder to fully update its parameters, where our V-Adapters are added in the last three layers for feature disentanglement. The results are presented in the second and third lines of Table 5, respectively. Moreover, since a single A100 GPU with 40GB memory can not afford these extra adapters or fully fine-tuned parameters with CLIP-large that contains 24 vision transformer (ViT) layers, we instead use CLIP-base with ViT-B/32 as its image encoder, and re-run baselines for a fair comparison. Regarding that some baselines with CLIP-large still perform worse than our methods with CLIP-base, we omit re-implementing them to save computation costs.

From Table 5, we can see that introducing more trainable parameters indeed achieves superior performance, in comparison with the vanilla models that only include 3 V-Adapters in the last three layers of the frozen image encoder. Especially, the fine-tuning method performs better. As a result, we implement our DCDA[PRG] and DCDA[PRG+N] with the whole image encoder fully tunable, the resulting models together with our V-Adapters achieve very competitive performance on C-GQA compared with the SOTA CAILA. Moreover, we also vary the number of transformer layers with V-Adapters inserted, starting from the top trans-

Models	S	U	H	AUC
Frozen Encoder + 3 V-Adapters (default)	34.8	23.4	21.6	6.9
Extra Adapters + 3 V-Adapters	38.8	26.6	23.8	8.7
Full Fine-Tuning + 3 V-Adapters	38.5	28.8	25.3	9.4
Full Fine-Tuning + 1 V-Adapters	38.9	26.4	24.6	8.8
Full Fine-Tuning + 2 V-Adapters	39.2	27.3	24.9	9.0
Full Fine-Tuning + 4 V-Adapters	38.8	25.6	24.2	8.5
Full Fine-Tuning + 6 V-Adapters	31.9	13.7	14.1	3.5

Table 5: Ablation on adding more trainable parameters in the vision encoder on C-GQA in *closed world*. All the results are tested with the “[PRG+N]” sampling method.

former layers, the results are as shown in the last four lines of Table 5. From Table 5, we have similar observations as in Figure 3, i.e., too few (e.g., only one) V-Adapter is not enough to disentangle the primitive features, while too many (e.g., 6) V-Adapters may overfit to disentangle the training data, resulting in poor generalization. To sum up, the fine-tuned image encoder and three V-adapters lead to a balance between adapting CLIP to the C-GQA dataset and disentangling its image features.

C. Supplementary Case Studies

We use examples from MIT-States to analyze the disentanglement of primitive features learned by CAILA and our DCDA (e.g., DCDA[PRG]), especially those visual ones. Specifically, we first randomly sample a set of seen and unseen compositions from the test set of MIT-States whose annotated attributes or objects have high diversity. Here, we use the number of associated objects (resp. attributes) to roughly measure the diversity of an attribute (resp. object) as a wider range of objects (resp. attributes) would lead to more diverse appearances of attributes (resp. objects). For example, in Figure 1, attribute *broken* describes 40 objects in the training set ranging from *car*, *drum* to *furniture* with different damaged states; similar to the object *knife* in Figure 4, which is paired with 9 attributes in the training set. In addition, we also manually select 2 ~ 3 attributes (resp. objects) whose associated objects (resp. attributes) are fewer but look greatly different, e.g., the attribute *worn* in Figure 1.

Then, for each sampled composition, we randomly extract at least 3 testing images and visualize their visually disentangled attribute and object representations learned by our DCDA and CAILA in Figure 1 and Figure 4, respectively, where different colors indicate different attribute or object labels. More specifically, for DCDA, we extract the features learned by our V-Adapters, i.e., $H_{* \rightarrow A}^v$ and $H_{* \rightarrow O}^v$; while for CAILA, we save the features learned by its attribute and object-specific vision encoding blocks.

From Figure 1 and Figure 4, it can be seen that the attribute embeddings or object embeddings learned by our model are clustered into different groups w.r.t different attributes or objects in each vector space. For example, in Figure 1, *broken car*, *broken drum* and *broken furniture* are in the same cluster in the attribute space, i.e., their learned attribute features are similar even though they show different *broken* state w.r.t different objects, similar to *curved knife* and *large knife* in Figure 4. Also, *broken car* is a seen composition, while *broken drum* and *broken furniture* are two

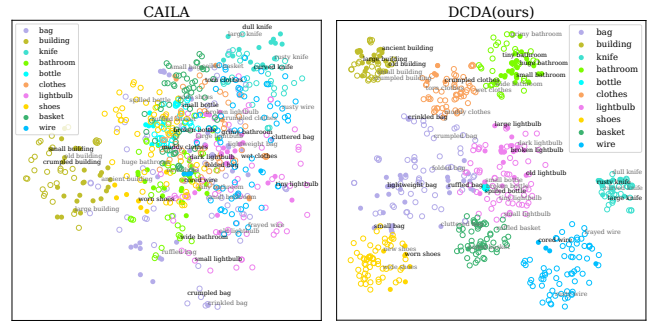


Figure 4: *t*-SNE visualizations of disentangled object representations of images in the test set of MIT-States, learned by CAILA and our DCDA. Solid and hollow circles represent images of seen and unseen compositions, respectively. Best viewed in color.

unseen compositions. However, the attribute embeddings as well as object embeddings learned by CAILA scatter in the attribute and object space, respectively. All of these illustrate that our DCDA captured similar visual features specific to each primitive, which is discriminative and generalizable.

Moreover, we also find that the attribute and object embeddings of the same composition are divided into different clusters with different neighbors in two spaces, for example, *large knife* and *dull knife* are two neighbors from the cluster of *knife* in the object space, while they fall into the clusters of *large* and *dull* in the attribute space with neighbors *large building* and *dull brass*, respectively. This indicates that our method indeed disentangles the attribute and object features into different representation spaces.